Article:
Guntakanti, U., Obireddy, S.R., Chintha, M. et al. (3 more authors) (2025) Ionically crosslinked composite gels containing amine-functionalized CoFe2O4 nanoparticles as a bioactive and pH-responsive drug delivery system. International Journal of Biological Macromolecules, 294. 139488. ISSN 0141-8130

https://doi.org/10.1016/j.ijbiomac.2025.139488

Ionically crosslinked composite gels containing amine-functionalized $CoFe_2O_4$ nanoparticles as a bioactive and pH-responsive drug delivery system

Ujwala Guntakanti[1], Sreekanth Reddy Obireddy[1], Madhavi Chintha[2], Karuna Sree Merugu[3], Wing-Fu Lai[4,*], Anitha Kowthalam[1,*]

1. Department of Chemistry, Sri Krishnadevaraya University, Ananthapur-515003,India.
2. Department of Polymer Science and Technology, Sri Krishnadevaraya University, Ananthapur-515003, India.
3. Department of Chemistry, GITAM School of Science, Bengaluru, Karnataka 562163, India
4. School of Food Science and Nutrition, University of Leeds, Leeds LS2 9JT, United Kingdom.

*E-mail: anitbios@gmail.com (AK); rori0610@graduate.hku.hk (WFL)

Abstract

Composite gels are a type of soft matter, which contains a continuous three-dimensional crosslinked network and has been embedded with non-gel materials. Compared to pure gels, composite gels show high flexibility and tunability in properties and hence have attracted extensive interest in applications ranging from cancer therapy to tissue engineering. In this study, we incorporated triethylenetetramine (TETA)-functionalized cobalt ferrite nanoparticles (ANPs) into a hydrogel consisting of sodium alginate (SA) and methyl cellulose (MC), and examined the resulting composite gels for controlled drug release. The structural, thermal, and morphological aspects of the composite gels were characterized to confirm successful nanoparticle incorporation. Swelling and degradation data demonstrated the pH-responsiveness and enhanced stability of the composite gels. Along with their controlled drug

release profiles and their ROS-generating capacity, our composite gels warrant further development as promising bioactive carriers for pharmaceutical applications.

Keywords: Cobalt ferrite nanoparticles; triethylenetetramine; sodium alginate; methyl cellulose; doxorubicin; gel beads; controlled release

1. Introduction

Increasing efforts have been put to integrate engineered nanoparticles (NPs) into pharmaceutical formulations over the last several decades [1-3]. These NPs, characterized by their augmented specific surface area and reactivity, present unique properties that hold the potential to enhance bioavailability and induce toxicity [4]. Despite limited data on their environmental impact, NPs, show promise in improving delivery of poorly water soluble drugs and enhancing bioavailability upon administration by enabling rapid absorption and target-specific delivery [5]. As far as carrier development is concerned, drug delivery systems generated by using biological macromolecules have been extensively developed [6-10]. Sodium alginate (SA) and cellulose derivatives [such as hydroxypropyl methyl cellulose (HPMC), carboxymethyl cellulose (CMC) and methyl cellulose (MC)] are some of the biomacromolecules recognized for good property tunability, high biocompatibility, high biodegradability, and excellent gelling capacity [11-13]; however, their wide application in drug delivery has been impeded by the comparatively poor mechanical strength of the gels formed and by the occurrence of burst drug release upon administration. To address this problem, in this study we incorporate cobalt ferrites ($CoFe_2O_4$) NPs into a SA/MC gel. These NPs have been found to exhibit not only strong antibacterial effects against *E. coli*, *S. aureus* and *B. cereus* but also anticancer properties in HEK-293 and MCF-7 cells [14, 15]. Due to their stability, nontoxicity and biocompatibility, $CoFe_2O_4$ NPs have been used in a range of

biological applications, ranging from diagnosis, hyperthermia and bioseparation to drug delivery [16-18].

In fact, metal oxide NPs have had a track record of use in drug carrier design. For instance, an earlier study has reported the use of nickel zinc ferrite-conjugated SA/poly(vinylpyrrolidone-co-vinyl acetate) beads as a carrier of DOX [19]. Amine-functionalized zinc ferrite NPs-loaded SA/CMC composite gels have also been used to delivery DOX to exert anticancer action against MCF7 cells [20]. Eslamiehei and coworkers have examined the characteristics of Co_3O_4 NPs and have found that the NPs possess antioxidant, antibacterial, and anticancer properties [21]. In this study, $CoFe_2O_4$ NPs are modified with triethylenetetramine (TETA) (which is a telomerase inhibitor with anti-angiogenesis effects [22] and can induce apoptosis in murine fibrosarcoma cells by activating the p38 mitogen-activated protein kinase (MAPK) pathway [23]) to generate amine-functionalized $CoFe_2O_4$ NPs (ANPs). By incorporating the ANPs into the gel matrix, we generate a bioactive drug carrier for the controlled release of doxorubicin (DOX). DOX is chosen as the drug model because it is renowned for inhibiting the rapid division of cancer cells [24, 25]. It is, therefore, a good agent to demonstrate the effectiveness of our reported system.

2. Material and Methods

2.1. Materials

MC, $CaCl_2$, and ethylene glycol were obtained from Merck, Mumbai, India. SA, cobalt (II) nitrate, iron (III) nitrate, and TETA were obtained from SD Fine chemicals, Mumbai, India. DOX was received from Aurbindo Pharma Ltd., Telangana, India.

2.2. Synthesis of ANPs

ANPs were synthesized from $Co(NO_3)_2 \cdot 6H_2O$ and $Fe(NO_3)_3 \cdot 9H_2O$ by using the hydrothermal method. 0.124g of $Co(NO_3)_2 \cdot 6H_2O$ and 0.344g of $Fe(NO_3)_3 \cdot 9H_2O$ were

dissolved in 20 mL of ethylene glycol under constant stirring. The pH of the resulting mixture was adjusted to 12 by using an NaOH (1M) solution and was heated to 110°C for one hour, followed by the addition of TETA. Afterwards, the solution was heated to 160°C and was kept at that temperature for 5 h. The generated ANPs were collected by centrifugation at 15000xg for 30 min, washed multiple times with ethanol to eliminate the solvent and any unbound TETA, and dried at 40°C.

2.3. Synthesis of composite gel beads

The composite gel beads were synthesized by ionic gelation. In brief, 200 mg of SA and 200 mg of MC were dissolved separately in 10 mL of millipore water and stirred overnight. The two solutions were mixed and stirred until a homogenous solution was obtained. Varying amounts of DOX and ANPs, as specified in Table 1, were added to the solution under constant stirring. The resulting mixture was added dropwise into a 5%(w/v) $CaCl_2$ solution to form composite gel beads, where were left for 40 min at ambient conditions to ensure complete crosslinking. The composite gel beads were collected, washed multiple times with millipore water, and air-dried overnight.

2.4. Structural characterization

Composite gel beads, $CoFe_2O_4$ NPs, SAMC, and DOX were examined by Fourier-transform infrared spectroscopy (FTIR) (Bomem MB-3000, Canada) in the 400–4000 cm^{-1} range. Data of X-ray diffraction (XRD) (Rigaku, Mini flex600, JAPAN) were collected at a scanning rate of 10°/min. Morphological analysis of the gel beads was conducted by scanning electron microscopy (SEM) (JOEL, IT500A, Japan). Transmission electron microscopy (TEM) (JEOL JEM 2100; JEOL, Japan) was adopted to determine the size of the NP.

2.5. Thermogravimetric analysis (TGA)

ANPs, DOX, SAMC, SAMC-ANPs-DOX, SAMC-DOX, and SAMC-ANPs were examined by using TGA (Q500, TA Instruments, USA). In brief, 5-7 mg of the sample were placed in an alumina crucible. Thermograms were recorded in the temperature range of 30-600 °C at a heating rate of 10 °C/min under a nitrogen atmosphere.

2.6. Determination of the loading efficiency (LE) and encapsulation efficiency (EE)

The LE and EE of the DOX-loaded composite gel beads was analyzed as previous described [26]. In brief, 5 mg of DOX-encapsulated composite gel beads were weighed and soaked for 24 hours in 20 mL of phosphate buffer saline (PBS). The beads were crushed and filtered after 15 minutes of sonication. An UV-Vis spectrophotometer was used to measure the absorbance of the filtrate at 481.5 nm. The LE and EE were determined using the equations adopted in an earlier study [27, 28].

2.7. *In vitro* release and kinetic studies

To determine the profiles of drug release, dissolution analysis was conducted. A suspension was prepared by dispersing 100 mg of the gel beads in 500 mL of PBS (pH 1.2, 6.4, and 7.4) at 37 °C. At regular intervals, 3 mL of the medium was withdrawn, with the volume being replenished with PBS. The sample was analyzed at 481.5 nm using a UV-Vis spectrophotometer. Release kinetics was determined by fitting the release profiles to various models, including zero-order, first-order, Higuchi, and Korsmeyer-Peppas models. Selection of the best-fit release mechanism model was based on the r^2values [29].

2.8. Examination of susceptibility to degradation

10 mg of the gel beads were weighted and dispersed in 5 mL of either PBS (pH 1.2, 6.4, or 7.4) or distilled water. The dispersions were incubated at either 37 °C or 4 °C. At regular intervals, the beads were retrieved and air-dried. The change in weight was determined to assess degradation.

2.9. Determination of cytotoxicity and bioactivity of gel beads

MCF-7 and MCF-10 cell lines were purchased from NCCS, Pune, India. The cells were cultured as previously described [30]. Cells were seeded in a 96-well plate at a density of 20,000 cells per well, and incubated for 24 hours at 37°C and 5% CO_2. During the experiment, the sample was introduced into each well at a specified concentration. After that, the plate was incubated at 37 °C and 5% CO_2 for 24 hours. The 3-(4,5-dimethylthiazol-2-yl)-2,5-diphenyltetrazolium bromide (MTT) reagent was added to each well at a concentration of 0.5 mg/mL. After three hours of incubation at 37 °C and 5% CO_2, the medium from each well was first removed, followed by the addition of 100 µL of DMSO to each well. Absorbance in each well at 570 nm was measured by using a microplate reader. Apart from the MTT assay, the ROS status of the treated cells was measured in accordance with the protocols delineated in our earlier studies [31-33].

2.10. Determination of cellular uptake

MCF-7 cells were seeded on a 6-well plate at a density of 2 x 10^5 cells per well, and incubated at 37°C and 5% CO_2. After 24 hours of incubation, the cells were treated with the sample (SAMC-ANPs, SAMC-DOX, and SAMC-ANPs-DOX) (which was pre-conjugated with fluorescein isothiocyanate (FITC) at a concentration of 10 µg/mL) at a concentration of 50 µg/mL in 2 mL of the culture medium. After incubation in CO_2 at 37°C for additional 24 hours, the culture medium was removed. The cells were washed with PBS. 500µL of a trypsin-EDTA solution were added to each well. The plate was incubated at 37°C for 4 minutes. After that, 2 mL of the culture medium were added, with the cells being harvested and put into a polystyrene tube. The tube was centrifuged for 5 minutes at 300 x g. The supernatant was decanted. The pellet was resuspended in 400µL of pre-warmed Dulbecco's phosphate-buffered saline (DPBS).

The cell suspension was analyzed by using a flow cytometer with 488 nm for excitation and 535 nm for detection.

2.11. Statistical analysis

All data were presented as the means ± standard deviations of triplicate experiments. Student's t-test was performed to assess statistical significance. Differences with a p-value < 0.05 were considered to be statistically significant.

3. Results and Discussion

3.1. Structural analysis

3.1.1. FTIR analysis

Interactions among DOX, ANPs and the gel matrix are examined by FTIR (Figure 1). The spectrum of DOX has peaks at 3326 cm^{-1} and 1731 cm^{-1}. These peaks are attributed to O-H or N-H and C=O vibrations, respectively. Peaks are also observed at 1589 cm^{-1} and 1388 cm^{-1}. They are assigned to N-H and O-H vibrations. Peaks at 1288 cm^{-1}, 1118 cm^{-1}, and 1081 cm^{-1} are assigned to C-O, C-N, and C-O vibrations. In the FTIR spectrum of $CoFe_2O_4$ NPs, peaks are found at 589 cm^{-1} (contributed to Fe^{3+}-O^{2-} complexation) and 427 cm^{-1} (contributed to M^{2+}-O^{2-} complexation, where M represents Fe and Co). Upon TETA-functionalizationnew peaks are found at 1127 cm^{-1} and 3346 cm^{-1}. This indicates the presence of TETA molecules on the NP surface.

In the spectrum of SAMC, distinctive peaks are found at 3431 cm^{-1} (assigned to O-H vibration), 1623 cm^{-1} (assigned to C=O vibration), and 1388 cm^{-1} (assigned to COO^- asymmetric stretching vibration). By comparing the spectrum of SAMC with that of SAMC-DOX, the band at 1623 cm^{-1} is found to be shifted to 1614 cm^{-1}, with a new peak (attributed to the C–N stretching vibration) at 957 cm^{-1} being observed. This shift, along with the emergence of a new peak, indicates the presence of drug molecules within the gel matrix. The spectrum of SAMC-

ANPs-DOX is similar to that of SA-MC-DOX, with a broad band at 591 cm^{-1} being found. This reveals the successful integration of ANPs into SAMC-ANPs-DOX. Peaks found in the spectrum of SAMC-ANPs are similar to those found in the spectrum of SAMC, with a new peak being observed at 589 cm^{-1}. This suggests successful incorporation of ANPs into the gel matrix. To confirm this, UV-visible absorption spectra are also collected (Figure 2). The absorption peak of DOX is observed at 485 nm. A similar peak is also noted in the spectrum of DOX-loaded gel beads. This confirms that DOX is successfully loaded into the gel beads.

3.1.2. XRD analysis

Interactions between different components in the composite gel beads are further examined by using XRD (Figure 3). The recorded 2θ angles (*viz.*, 18.2°, 30°, 35.4°, 37.05°, 43°, 53.4°, and 56.9°) found in the pattern of $CoFe_2O_4$ NPs correspond to crystallographic planes (111), (220), (311), (222), (400), (422), (511), and (440), respectively. These peaks align with Joint Committee on Powder Diffraction Standards (JCPDS) No. 22-1086 [34] and are consistent with prior findings made by Malinowska and co-workers [35]. The XRD pattern of DOX exhibits peaks in the 10.0°-25.0° 2θ range. Such peaks are absent in the XRD patterns of SAMC-DOX and SAMC-NPs-DOX. This suggests uniform dispersion of DOX molecules within the gel matrix at the molecular level. The XRD pattern of SAMC-NPs is highly similar to that of $CoFe_2O_4$NPs. All these evidence successful integration of $CoFe_2O_4$ NPs into the gel matrix.

3.2. Thermal analysis

TGA curves of gel beads and DOX are presented in Figure 4. No remarkable mass loss is found in the curve of DOX until 191 °C is reached. After that, a gradual mass loss is observed. A distinct peak at 257 °C indicates a significant mass loss. This is attributed to the decomposition of DOX. In the TGA curve of ANPs, minimal weight loss is detected, with only 13.3% of mass

loss being observed over the temperature range of 35-600 °C. This shows the intrinsic thermal stability of the ANPs. After incorporation of ANPs into the gel matrix, the mass loss found in the curves of SAMC-ANPs-DOX and SAMC-ANPs is significantly lower than that found in the curve of SAMC. This suggests that the presence of ANPs enhances the thermal stability of the SAMC gel.

3.3. Morphological analysis

Morphological analysis of the composite gel beads is examined by SEM (Figure 5). The composite gel beads exhibit a distinctive spherical shape with a rough surface. Comparing SAMC-DOX (Figure 5a) with SAMC-ANPs-DOX (Figure 5b), the outer surface of SAMC-DOX appears to be smoother while SAMC-ANPs-DOX displays a rougher surface. This is attributed to the incorporation of ANPs, leading to an increase in surface roughness and porosity. A similar phenomenon is observed in the micrographs of SAMC-ANPs (Figure 5c). The integration of ANPs imparts a characteristic texture to the surface of SAMC-ANPs gel beads. The average size of the composite gel beads is found by TEM to be in the range of 600-900 μm; whereas that of the ANPs is estimated to be around 15-30 nm (Figure 5d).

3.4. Swelling capacity

The swelling characteristics of the gel beads is studied at pH 2.0 and 7.4 (Figure 6). Swelling capacity at pH 7.4 was found to be higher than that at pH 2.0. This is attributed to the fact that, in the gel matrix, interactions of -COOH groups decrease at pH 7.4. This allows PBS to enter more easily, leading to a higher degree of swelling. The degree of swelling exhibited by SAMC-DOX is lowered than that of SAMC-ANPs-DOX. This can be explained by the fact that incorporation of ANPs induces increased porosity of the gel matrix to increase the swelling capacity. The results reveal the role of ANPs in modulating the swelling behavior of gel beads.

Such tunability in swelling capacity is anticipated to enable the developed beads to be potentially used in controlled drug delivery.

3.5. Drug loading and *in vitro* release

The LE and EE of SAMC-DOX are 22.5% and 70.9%, respectively. Those of SAMC-ANPs-DOX are 25.7 % and 73.5%, respectively. The EE of SAMC-ANPs-DOX is higher than that of SAMC-DOX because incorporation of ANPs into the gel not only increases the volume of pores and voids in the gel beads but also promotes interactions (e.g., hydrogen bonding and electrostatic attractions) between DOX and ANPs. All these, increase the efficiency in drug loading. This finding is consistent with that of Gholamali *et al.*[36], who found that hydrogels exhibit higher drug loading capacity upon NP incorporation.

In vitro release studies of our composite gel beads are conducted in different pH conditions (pH 2.0, 6.4, and 7.4), with the results being presented in Figure 7. At pH 7.4, minimal ionic interactions experienced by the COO^- groups in the gel. This increases the rate of drug release. The release rate observed at pH 6.4 is lower than that at pH 7.4. This is because an increase in the extent of ionic interactions in the gel hinder diffusion of the release medium into the gel. Ionic interactions in the gel are most significant at pH 2.0, at which the rate of drug release is highest among all pH conditions examined. The drug release profiles of different gel beads are fitted into various kinetic models, with the r^2 values obtained being presented in Table 2. The release kinetics of the gel beads fit the first-order model and the Higuchi model well. The release mechanism, therefore, involves initial uptake of the release medium into the gel beads, followed by diffusion of DOX into the external environment. The release rates of the beads show a direct correlation with the DOX content. To understand the release mechanism of the beads, the Korsmeyer-Peppas equation is applied to the release data (Table 2). The n values fall within the range of 0.405 to 0.592, indicating a non-Fickian diffusion pattern in drug release.

3.6. Degradation studies

Degradation studies of the gel beads are carried out at various pH (7.4, 6.4, and 2.0) and temperatures (37 ºC and 4 ºC) (Figure 8). The beads show a faster degradation rate when the pH of the media increases. This is evident at pH 7.4. Both SAMC and SAMC-ANPs exhibit a degradation rate higher than that at pH 2.0. This is because at pH 7.4, SA has higher solubility. This makes beads more susceptible to degradation. Furthermore, PBS at pH 7.4 contains Na^+ ions, which exchange with Ca^{2+} ions of the gel beads, weakening the matrix structure and leading to a higher rate of degradation [37]. Contrary to the case above, at pH 2.0, gel beads are more resistant to degradation because of the low solubility of SA.

In addition to pH, temperature affects the rate of degradation. Compared to 4°C, 37°C leads to more significate degradation experienced by the gel beads. This is because, as temperature increases, the gel matrix has more interaction with solvent molecules, leading to greater solvent absorption and faster degradation. The effect of ANPs on the degradation of the gel beads has also been examined in this study. The degradation rate of SAMC is higher than that of SAMC-ANPs. This difference is attributed to the formation of rigid networks led by hydrogen bonding and by electrostatic attractions between ANPs and the gel matrix. All these indicate that incorporation of ANPs into the gel matrix improves the mechanical strength of the gel and render the gels more susceptible to degradation.

Morphological analysis of the gels during degradation has been monitored by SEM (Figure 10). After 24 hours of degradation at pH 7.4, changes in the outer surface of the gel beads are not significant. However, after 6 days and 14 days of degradation, the outer structure becomes rough, fractured, and porous. Compared to degradation at pH 7.4, changes in the outer structure of the gel beads degraded at pH 6.4 are less significant. This confirms that degradation of the gel beads is more significant at pH 7.4 than at pH 6.4.

3.7. Cytotoxicity and ROS-generating capacity

The cytotoxicity and corresponding IC_{50} values of DOX, SAMC-DOX, SAMC-ANPs-DOX, and SAMC-ANPs are presented in Figure 11. Based on the result of the MTT assay, the viability of MCF-10A cells treated with SAMC (at a concentration of 100 μg/mL) exceeds 98% and those treated with ANPs (at a concentration of 100 μg/mL) exceeds 80%. This suggests that the cytotoxicity of both SAMC and ANPs is not significant. On the other hand, MCF-7 cells treated with DOX, SAMC-DOX and SAMC-ANPs-DOX show a decline in viability. Yet, comparing with those treated with DOX alone, the decline in the viability of cells treated with SAMC-DOX and SAMC-ANPs-DOX is less significant. This is attributed to sustained release of DOX from the gel beads, less to a lower concentration of DOX in the culture medium during cell treatment. Here it is worth noting that SAMC-ANPs alone also display cytotoxic effects. This can be explained by the fact that TETA is a telomerase inhibitor by itself. Owing to the crucial role played by telomerase in mediating cellular immortalization and tumorigenesis [38, 39], the TETA moiety of ANPs in the beads may inhibit tumor growth. In addition, ANPs exhibit reactive oxygen species (ROS)-generating capacity. A significant increase in the ROS level in MCF-7 cells upon treatment with ANPs, as illustrated in Figure 11C, supports this notion and aligns with other reported findings made on NP-based carriers in the literature [40-42].

Cellular uptake of DOX and/or ANPs released from SAMC-ANPs-DOX and SAMC-DOX is confirmed by flow cytometry (Figure 12), in which the fluorescence intensity of single-cell emission is used to quantify the amounts of ANPs and DOX internalized by the cell. As shown in Figure 12, the fluorescence intensity of the cells increases significantly after treatment with SAMC-ANPs-DOX, SAMC-DOX or SAMC-ANPs. SAMC-ANPs and SAMC-DOX exhibit 19% and 84.16% of cellular uptake in MCF-7 cells, respectively; whereas the cellular uptake experienced by SAMC-ANPs-DOX is as high as 98.85%. This suggests that ANPs and DOX

released from SAMC-ANPs-DOX may have a synergistic effect in facilitating cellular uptake of the beads, though further studies are needed to elucidate the underlying mechanism.

4. Conclusion

Composite gels generally show higher tunability in properties than pure gels, thereby rendering their drug delivery performance capable of being tailored to meet the needs of different applications. In this study, we have designed bioactive and pH-responsive composite gels by incorporating ANPs into the SA/MC gel matrix. ANP incorporation has been found to improve thermal stability of the gel and make the gel more resistant to degradation. In addition, DOX and ANPs have shown synergistic effects in mediating cellular uptake of the gel beads. Here it is worth mentioning that this study has several limitations. Firstly, precise control over the polydispersity and size of SAMC-ANPs-DOX beads is challenging. More sophisticate techniques (e.g., microfluidic technologies) in manipulating droplets may be adopted to help narrow down variations in the size and shape of the generated beads in the future. Secondly, the loading capacity of the gel beads is comparatively low. Further optimization of the drug loading process may help increase the efficiency. Finally, till now the drug delivery performance of the gel beads has only been tested *in vitro*. Preclinical trials are needed to verify the pharmacokinetic profiles of the beads upon administration into a living body. Despite the limitations as mentioned above, regarding the favorable properties (e.g., high drug release sustainability, good cellular uptake efficiency and intrinsic ANP-associated ROS-generating capacity) of the gel beads reported in this study, our beads warrant further development as a promising carrier for treatment development.

Conflict of Interests

The authors declare no conflict of interest

References

[1] W.-F. Lai, H.C. Shum, A stimuli-responsive nanoparticulate system using poly (ethylenimine)-graft-polysorbate for controlled protein release, Nanoscale, 8 (2016) 517-528.

[2] W.-F. Lai, W.-T. Wong, Design of polymeric gene carriers for effective intracellular delivery, Trends Biotechnol. 36 (2018) 713-728.

[3] W.-F. Lai, Z.-D. He, Design and fabrication of hydrogel-based nanoparticulate systems for in vivo drug delivery, J. Control. Release 243 (2016) 269-282.

[4] L. Xuan, Z. Ju, M. Skonieczna, P.K. Zhou, R. Huang, Nanoparticles-induced potential toxicity on human health: Applications, toxicity mechanisms, and evaluation models, MedComm (2020), 4 (2023) e327.

[5] A.A. Yetisgin, S. Cetinel, M. Zuvin, A. Kosar, O. Kutlu, Therapeutic nanoparticles and their targeted delivery applications, Molecules 25 (2020) 2193.

[6] W.-F. Lai, C. Hu, G. Deng, K.-H. Lui, X. Wang, T.-H. Tsoi, S. Wang, W.-T. Wong, A biocompatible and easy-to-make polyelectrolyte dressing with tunable drug delivery properties for wound care, Int. J. Pharm. 566 (2019) 101-110.

[7] W.-F. Lai, H.C. Shum, Hypromellose-graft-chitosan and its polyelectrolyte complex as novel systems for sustained drug delivery, ACS Appl. Mater. Interfaces 7 (2015) 10501-10510.

[8] W.-F. Lai, E.M. Huang, W.-T. Wong, A gel-forming clusteroluminogenic polymer with tunable emission behavior as a sustained-release carrier enabling real-time tracking during bioactive agent delivery, Appl. Mater. Today 21 (2020) 100876.

[9] W.-F. Lai, O.S. Reddy, L. Law, H. Wu, W.-T. Wong, A self-indicating and antibacterial gelatine–chitosan blended hydrogel enabling real-time quality control and sustained bioactive agent delivery, RSC Adv. 13 (2023) 11865-11873.

[10] W.-F. Lai, A.S. Susha, A.L. Rogach, Multicompartment microgel beads for co-delivery of multiple drugs at individual release rates, ACS Appl. Mater. Interfaces 8 (2016) 871-880.

[11] S.R. Obireddy, S. Bellala, M. Chintha, A. Sake, S.M.C. Subbarao, W.-F. Lai, Synthesis and properties of alginate-based nanoparticles incorporated with different inorganic nanoparticulate modifiers for enhanced encapsulation and controlled release of favipiravir, Arab. J. Chem., 16 (2023) 104751.

[12] O.S. Reddy, M. Subha, T. Jithendra, C. Madhavi, K.C. Rao, Fabrication and characterization of smart karaya gum/sodium alginate semi-IPN microbeads for controlled release of D-penicillamine drug, Polym. Polym. Compos. 29 (2021) 163-175.

[13] W.-F. Lai, O.S. Reddy, D. Zhang, H. Wu, W.-T. Wong, Cross-linked chitosan/lysozyme hydrogels with inherent antibacterial activity and tuneable drug release properties for cutaneous drug administration, Sci. Technol. Adv. Mater. 24 (2023) 2167466.

[14] J. Panda, S. Das, S. Kumar, B. Tudu, R. Sarkar, Investigation of antibacterial, antioxidant, and anticancer properties of hydrothermally synthesized cobalt ferrite nanoparticles, Appl. Phys. A 128 (2022) 562.

[15] S. Fiaz, M.N. Ahmed, I. ul Haq, S.W.A. Shah, M. Waseem, Green synthesis of cobalt ferrite and Mn doped cobalt ferrite nanoparticles: Anticancer, antidiabetic and antibacterial studies, J. Trace Elem. Med. Biol. 80 (2023) 127292.

[16] S. Al Lehyani, R. Hassan, A. Alharbi, T. Alomayri, H. Alamri, Magnetic hyperthermia using cobalt ferrite nanoparticles: the influence of particle size, Int. J. Adv. Technol. 8 (2017) 567-579.

[17] E. Fantechi, C. Innocenti, M. Albino, E. Lottini, C. Sangregorio, Influence of cobalt doping on the hyperthermic efficiency of magnetite nanoparticles, J. Magn. Magn. Mater. 380 (2015) 365-371.

[18] C. Dey, A. Ghosh, M. Ahir, A. Ghosh, M.M. Goswami, Improvement of anticancer drug release by cobalt ferrite magnetic nanoparticles through combined pH and temperature responsive technique, ChemPhysChem 19 (2018) 2872-2878.

[19] E. Venkata Ramana, G. Ujwala, S. Shahinshavali, S. Abdul Mathin, O. Sreekanth Reddy, Naseem, Development and Evaluation of pH-Responsive Microbeads Incorporated with Nickel Zinc Ferrite Nanoparticles for Controlled Release of Doxorubicin, ChemistrySelect 9 (2024) e202402227.

[20] S. Bellala, K. Viswanathan, U. Guntakanti, A. Kowthalam, S.S. Han, M.R. Kummara, S.R. Obireddy, W.-F. Lai, Composite Microgels Loaded with Doxorubicin-Conjugated Amine-Functionalized Zinc Ferrite Nanoparticles for Stimuli-Responsive Sustained Drug Release, Int. J. Nanomed. 19 (2024) 5059-5070.

[21] F. Momen Eslamiehei, M. Mashreghi, M.M. Matin, Advancing colorectal cancer therapy with biosynthesized cobalt oxide nanoparticles: a study on their antioxidant, antibacterial, and anticancer efficacy, Cancer Nanotechnol. 15 (2024) 22.

[22] K. Ganesan, B. Xu, Telomerase Inhibitors from Natural Products and Their Anticancer Potential, Int. J. Mol. Sci. 19 (2018) 13.

[23] S. Kadowaki, D. Endoh, T. Okui, M. Hayashi, Trientine, a copper-chelating agent, induced apoptosis in murine fibrosarcoma cells by activation of the p38 MAPK pathway, J. Vet. Med. Sci. 71 (2009) 1541-1544.

[24] H. Ma, Y. Liu, M. Shi, X. Shao, W. Zhong, W. Liao, M.M. Xing, Theranostic, pH-responsive, doxorubicin-loaded nanoparticles inducing active targeting and apoptosis for advanced gastric cancer, Biomacromolecules 16 (2015) 4022-4031.

[25] K. Ali, B. Jiang, W. Ashraf, A. Bin Tahir, F. ul Haq, Improving the functional characteristics of thymol-loaded pullulan and whey protein isolate-based electrospun nanofiber, Food Biosci. 57 (2024) 103620.

[26] A.A. Ezhilarasi, J.J. Vijaya, K. Kaviyarasu, M. Maaza, A. Ayeshamariam, L.J. Kennedy, Green synthesis of NiO nanoparticles using Moringa oleifera extract and their biomedical

applications: Cytotoxicity effect of nanoparticles against HT-29 cancer cells, J. Photochem. Photobiol. B 164 (2016) 352-360.

[27] W.F. Lai, R. Deng, T. He, W.T. Wong, A Bioinspired, Sustained-Release Material in Response to Internal Signals for Biphasic Chemical Sensing in Wound Therapy, Adv. HealthC. Mater. 10 (2021) 2001267.

[28] G. Ujwala, C. Madhavi, O.S. Reddy, M. Subha, K. Anitha, Synthesis and characterization of polymeric microbeads loaded with lithium cobalt oxide nanoparticles for drug delivery and antibacterial applications, J. Coastal Life Med. 10 (2022) 515-524.

[29] R.T. Stiepel, E.S. Pena, S.A. Ehrenzeller, M.D. Gallovic, L.M. Lifshits, C.J. Genito, E.M. Bachelder, K.M. Ainslie, A predictive mechanistic model of drug release from surface eroding polymeric nanoparticles, J. Control. Release 351 (2022) 883-895.

[30] D. Fischer, M. Seifert, S. Becker, D. Lüdders, T. Cordes, J. Reichrath, M. Friedrich, 25-hydroxyvitamin D3 1α-hydroxylase splice variants in breast cell lines MCF-7 and MCF-10, Cancer Genomics & Proteomics 4 (2007) 295-300.

[31] B. Adilakshmi, O.S. Reddy, D. Hemalatha, K.S.K. Rao, W.-F. Lai, ROS-generating poly (Ethylene Glycol)-Conjugated Fe3O4 nanoparticles as cancer-targeting sustained release carrier of doxorubicin, Int. J. Nanomed. 17 (2022) 4989.

[32] S.R. Obireddy, W.-F. Lai, Multi-component hydrogel beads incorporated with reduced graphene oxide for ph-responsive and controlled co-delivery of multiple agents, Pharmaceutics 13 (2021) 313.

[33] G. Ujwala, C. Madhavi, O.S. Reddy, R.R. Raju, T. Kalyankar, K. Anitha, Development and characterization of sodium alginate-g-poly (acrylic acid-co-2-acrylamido-2-methyl-1-propane sulfonic acid)/locust bean gum microbeads containing nickel ferrite nanoparticles for pH-responsive release of doxorubicin, Mater. Today: Proc. 92 (2023) 899-905.

[34] S. Rohilla, S. Kumar, P. Aghamkar, S. Sunder, A. Agarwal, Investigations on structural and magnetic properties of cobalt ferrite/silica nanocomposites prepared by the coprecipitation method, J. Magn. Magn. Mater. 323 (2011) 897-902.

[35] I. Malinowska, Z. Ryżyńska, E. Mrotek, T. Klimczuk, A. Zielińska-Jurek, Synthesis of CoFe2O4 nanoparticles: the effect of ionic strength, concentration, and precursor type on morphology and magnetic properties, J. Nanomater. 2020 (2020) 9046219.

[36] I. Gholamali, M. Yadollahi, Doxorubicin-loaded carboxymethyl cellulose/Starch/ZnO nanocomposite hydrogel beads as an anticancer drug carrier agent, Int. J. Biol. Macromol. 160 (2020) 724-735.

[37] M. Bhansali, N. Dabholkar, P. Swetha, S.K. Dubey, G. Singhvi, Chapter 18 - Solid Oral Controlled-Release Formulations, in: A.T. Azar (Ed.) Modeling and Control of Drug Delivery Systems, Academic Press 2021, pp. 313-331.

[38] J. Liu, L. Guo, F. Yin, X. Zheng, G. Chen, Y. Wang, Characterization and antitumor activity of triethylene tetramine, a novel telomerase inhibitor, Biomed. Pharmacother. 62 (2008) 480-485.

[39] J. Lu, Triethylenetetramine pharmacology and its clinical applications, Mol. Cancer Ther. 9 (2010) 2458-2467.

[40] S. Fu, R. Yang, J. Ren, J. Liu, L. Zhang, Z. Xu, Y. Kang, P. Xue, Catalytically active CoFe2O4 nanoflowers for augmented sonodynamic and chemodynamic combination therapy with elicitation of robust immune response, Acs Nano 15 (2021) 11953-11969.

[41] S. Klein, M. Kızaloğlu, L. Portilla, H. Park, T. Rejek, J. Hümmer, K. Meyer, R. Hock, L.V. Distel, M. Halik, Enhanced in vitro biocompatibility and water dispersibility of magnetite and cobalt ferrite nanoparticles employed as ROS formation enhancer in radiation cancer therapy, Small 14 (2018) 1704111.

[42] M.M. Naik, H.B. Naik, N. Kottam, M. Vinuth, G. Nagaraju, M. Prabhakara, Multifunctional properties of microwave-assisted bioengineered nickel doped cobalt ferrite nanoparticles, J. Sol-Gel Sci. Technol. 91 (2019) 578-595.

Figures

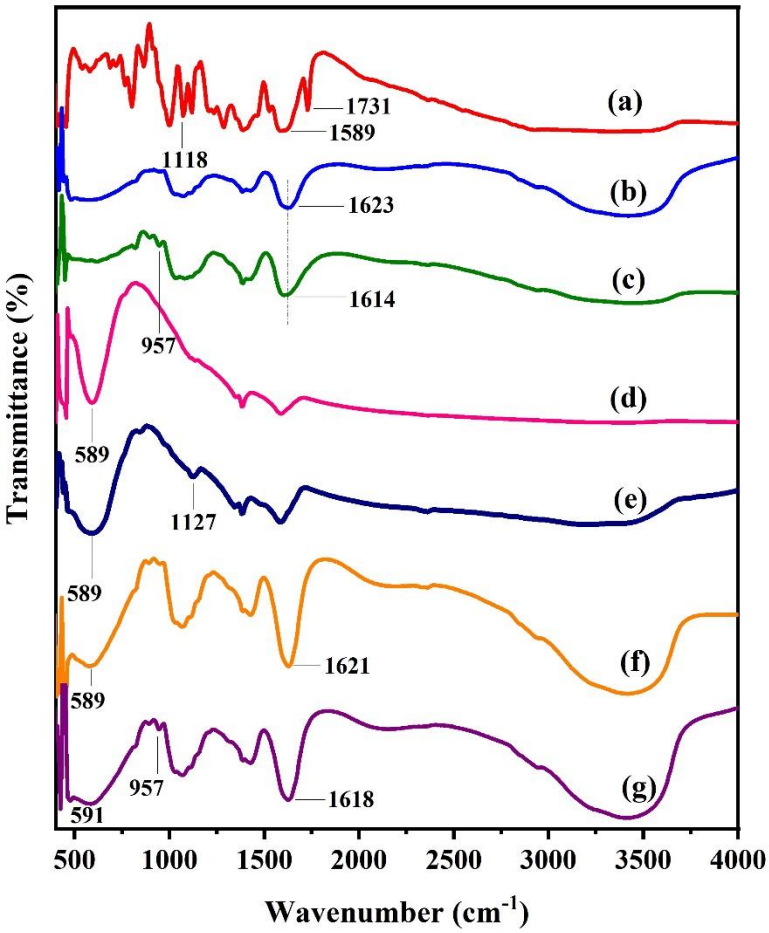

Figure 1 FTIR spectra of (a) DOX, (b) SAMC, (c) SAMC-DOX, (d) $CoFe_2O_4$ NPs, (e) ANPs, (f) SAMC-ANPs and (g) SAMC-ANPs-DOX.

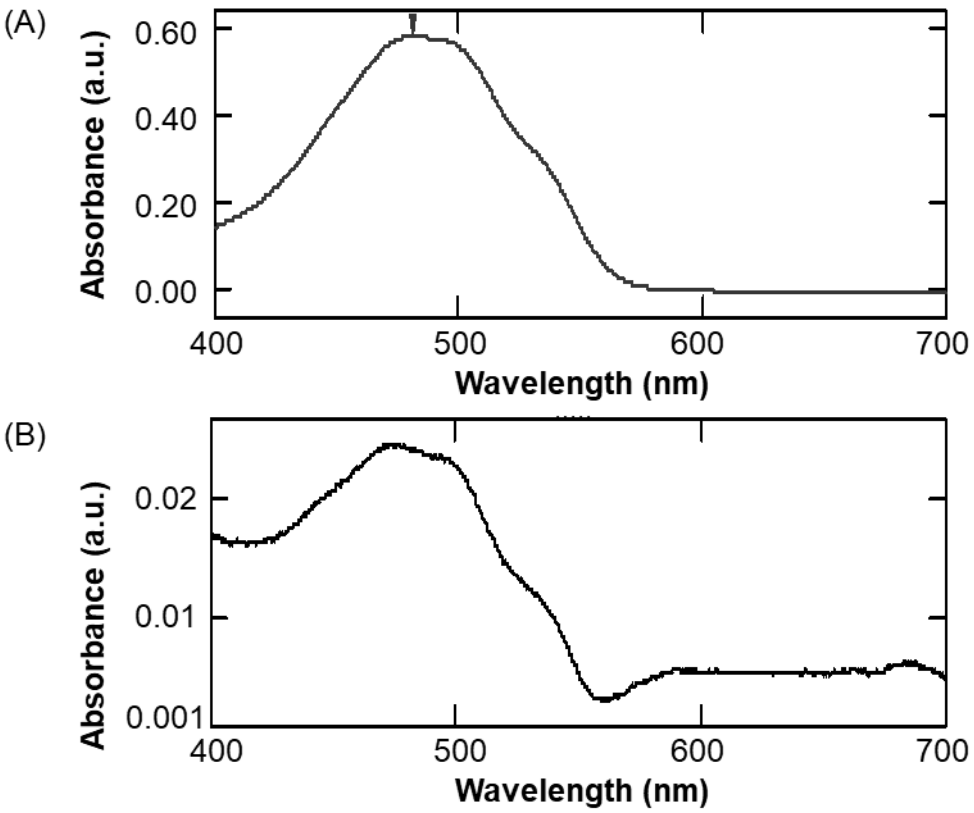

Figure 2. UV-visible absorption spectra of (A) DOX and (B) SAMC-DOX.

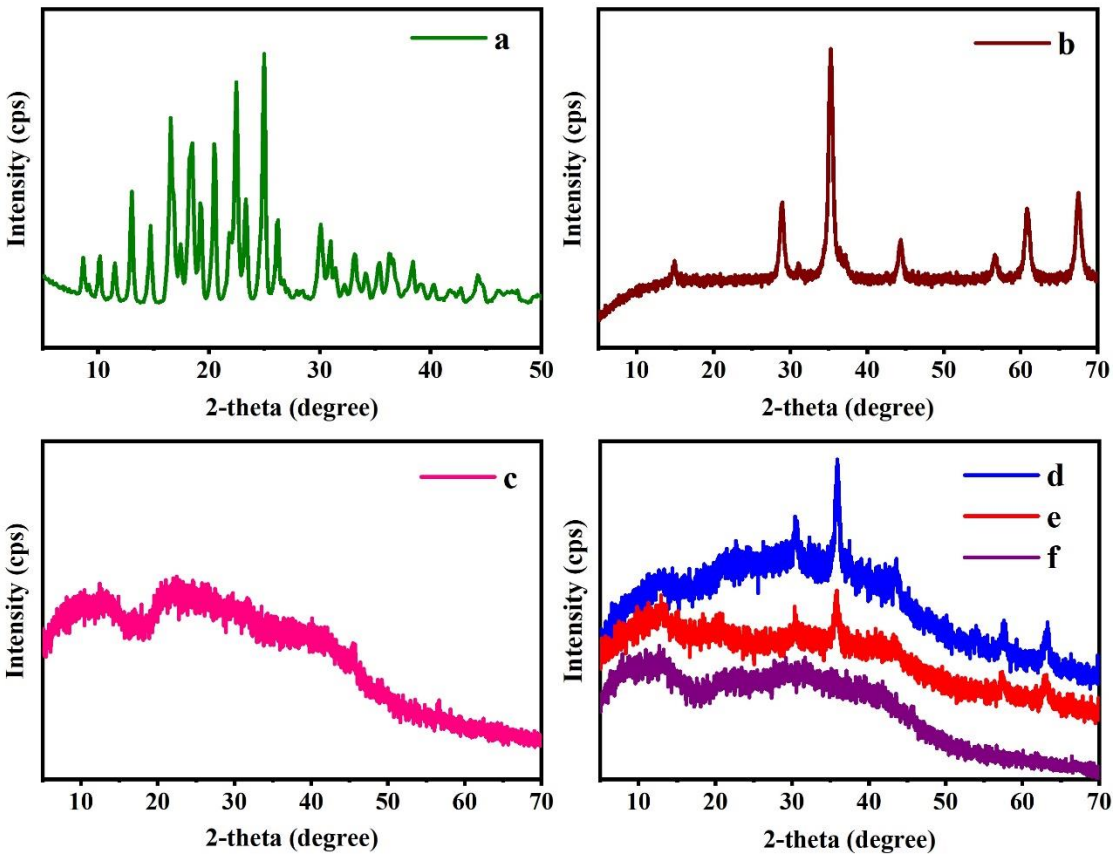

Figure 3. XRD patterns of (a) DOX, (b) $CoFe_2O_4$ NPs, (c) SAMC, (d) SAMC-DOX, (e) SAMC-ANPs-DOX, and (f) SAMC-ANPs

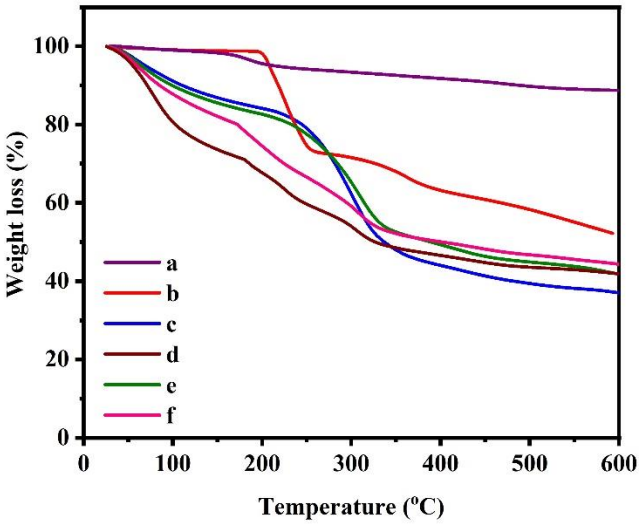

Figure 4. TGA graphs of (a) ANPs, (b) DOX, (c) SAMC, (d) SAMC-ANPs-DOX, (e) SAMC-DOX, and (f) SAMC-ANPs.

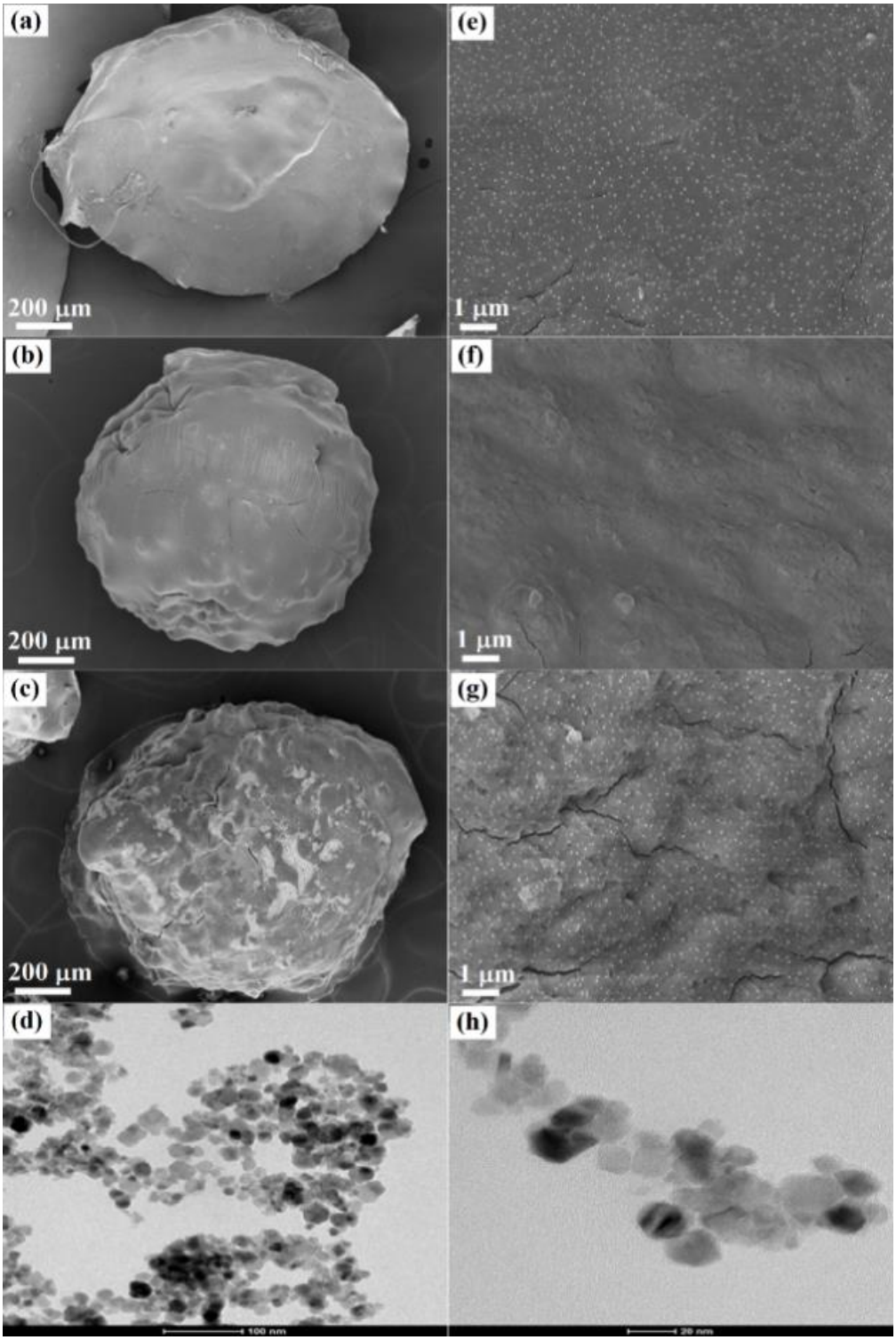

Figure 5. SEM micrographs of (a, e) SAMC-DOX, (b, f) SAMC-ANPs-DOX, and (c, g) SAMC-ANPs. (d, h) TEM micrographs of $CoFe_2O_4$ NPs.

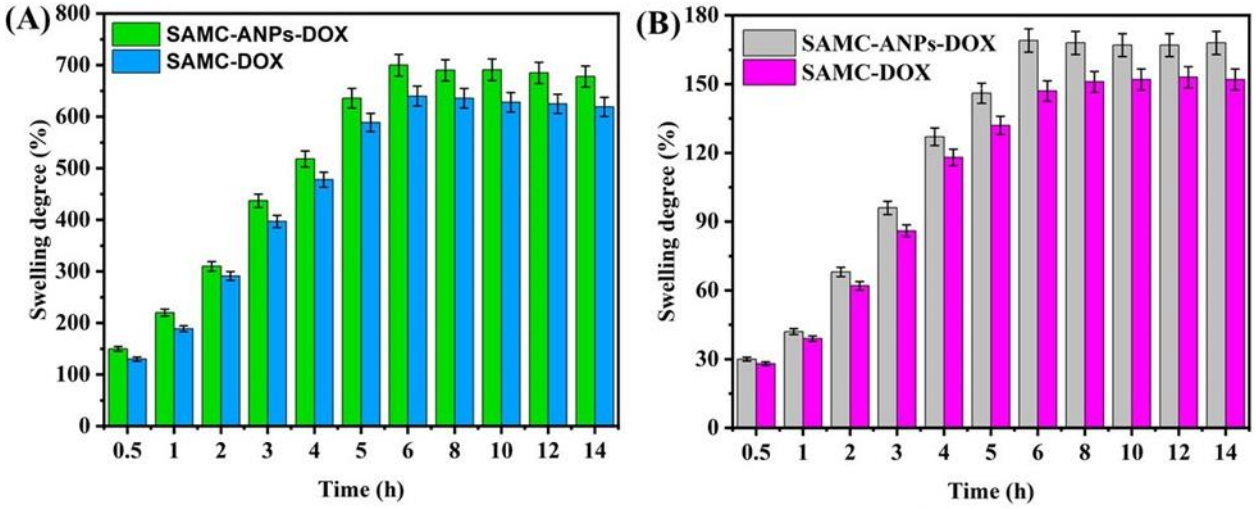

Figure 6. Swelling capacity of SAMC-ANPs-DOX and SAMC-DOX at (A) pH 7.4, (B) 2.0.

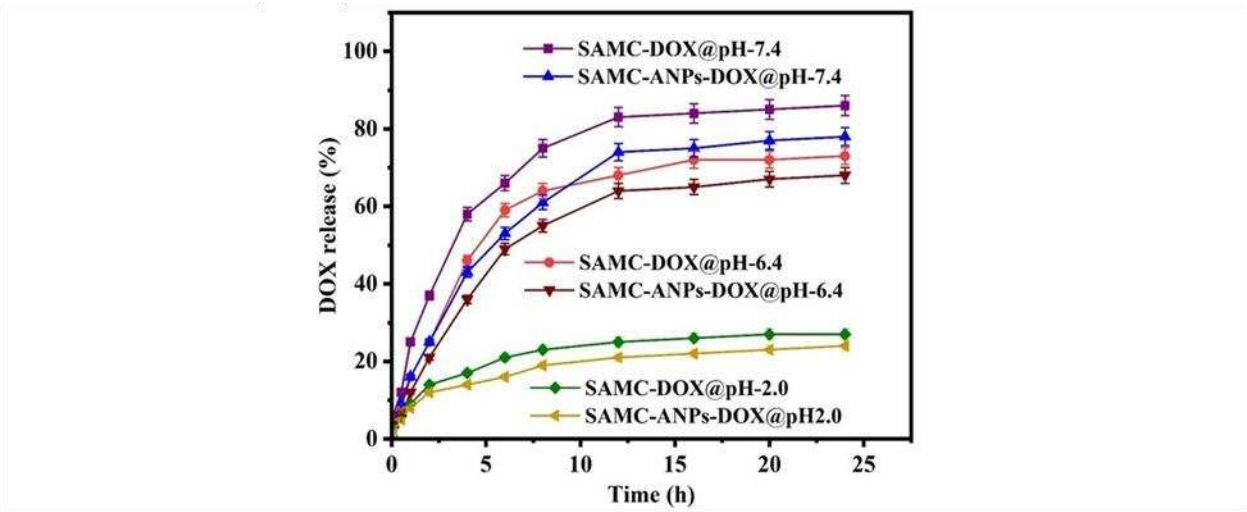

Figure 7. Drug release profiles of SAMC-DOX and SAMC-ANPs-DOX at pH 2.0, 6.4 and 7.4 at 37 °C.

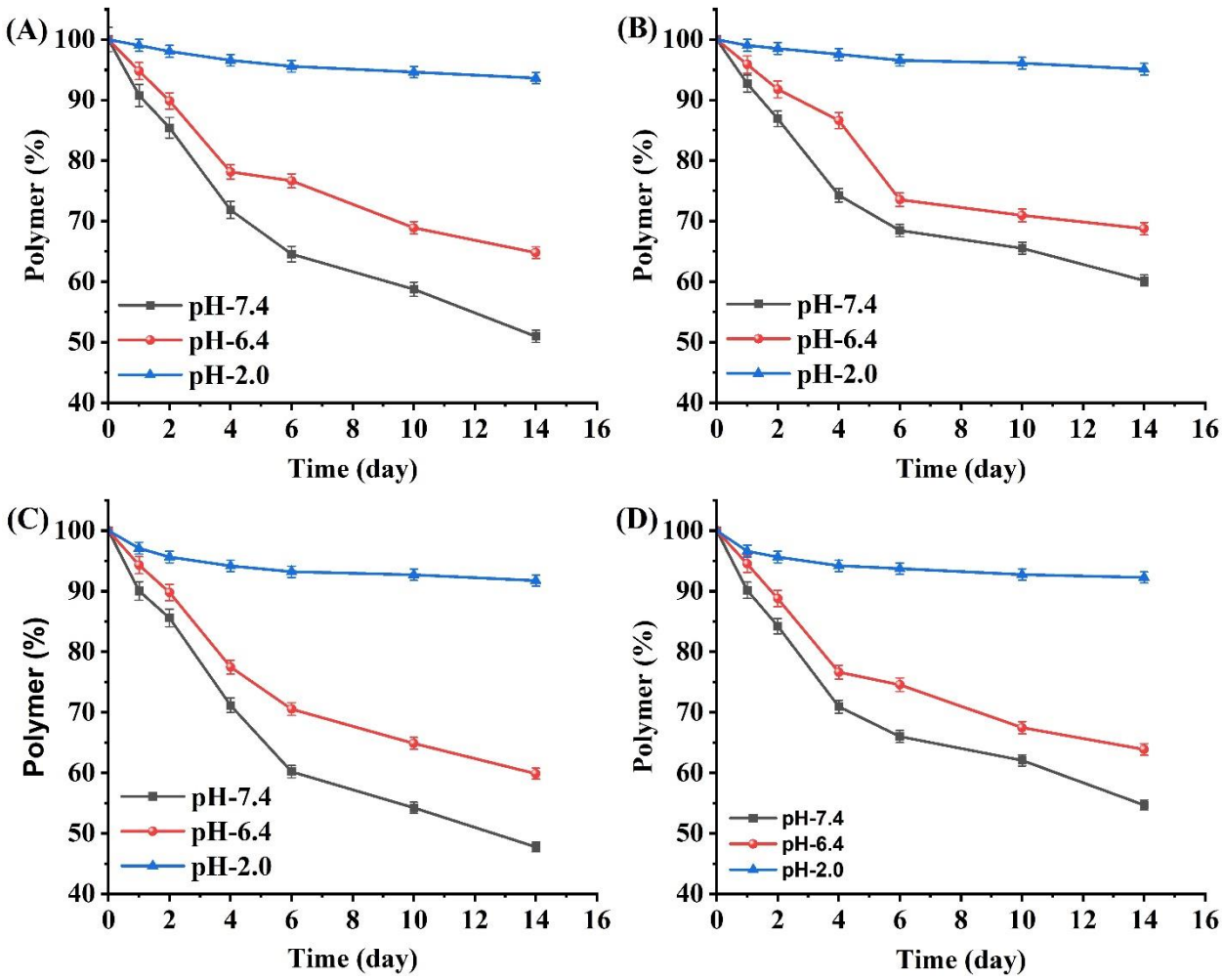

Figure 8. Degradation of (A, B) SAMC-ANPs and (C, D) SAMC in PBS at (A, C) 37 ^{0}C and (B, D) 4 ^{0}C.

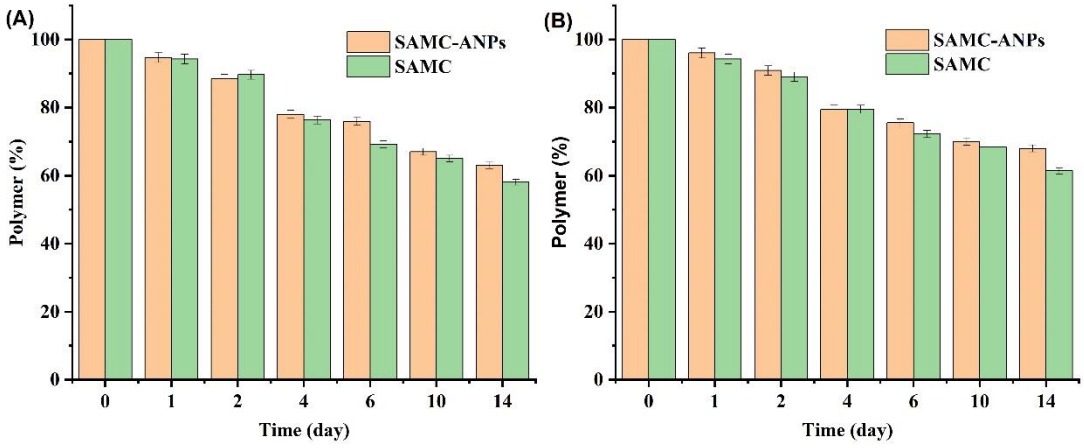

Figure 9. Degradation studies of SAMC-ANPs and SAMC in water at (A) 37 ºC and (B) 4 ºC

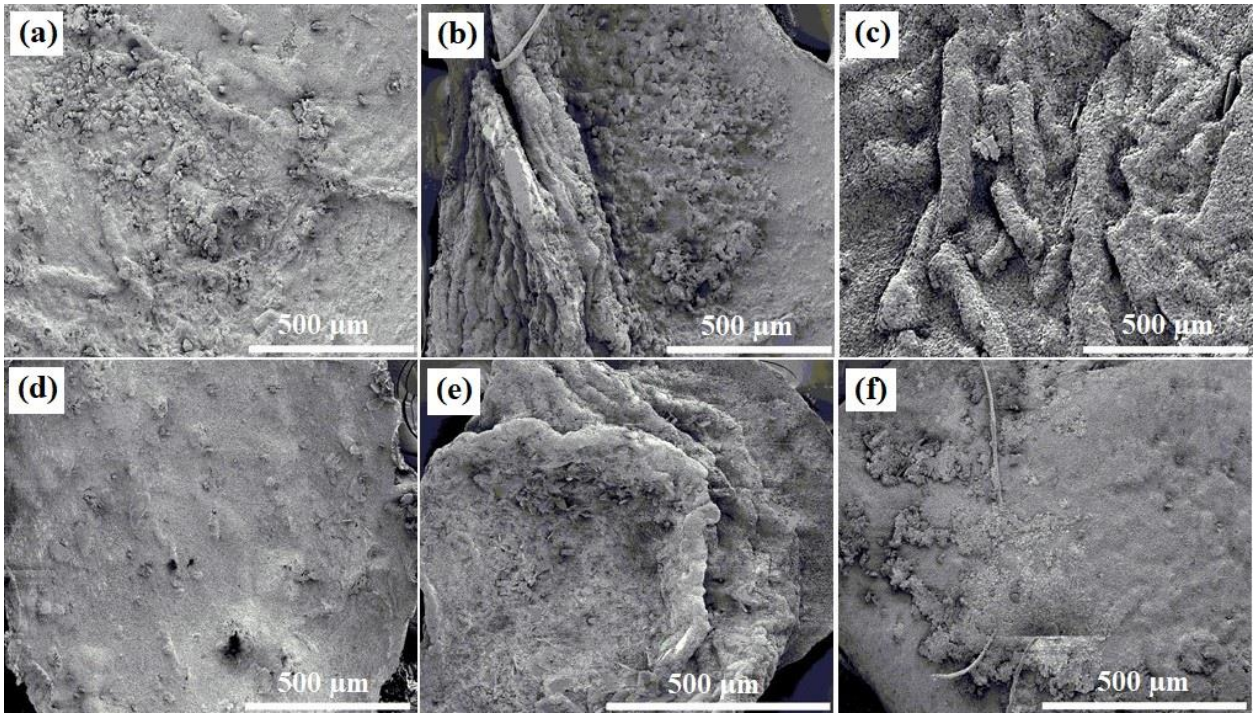

Figure 10. SEM micrographs of SAMC upon degradation at (a- c) pH 7.4 and (d-f) pH 6.4. The images were taken (a, d) 1 day, (b, e) 6 days, and (c, f) 14 days after the onset of the degradation study.

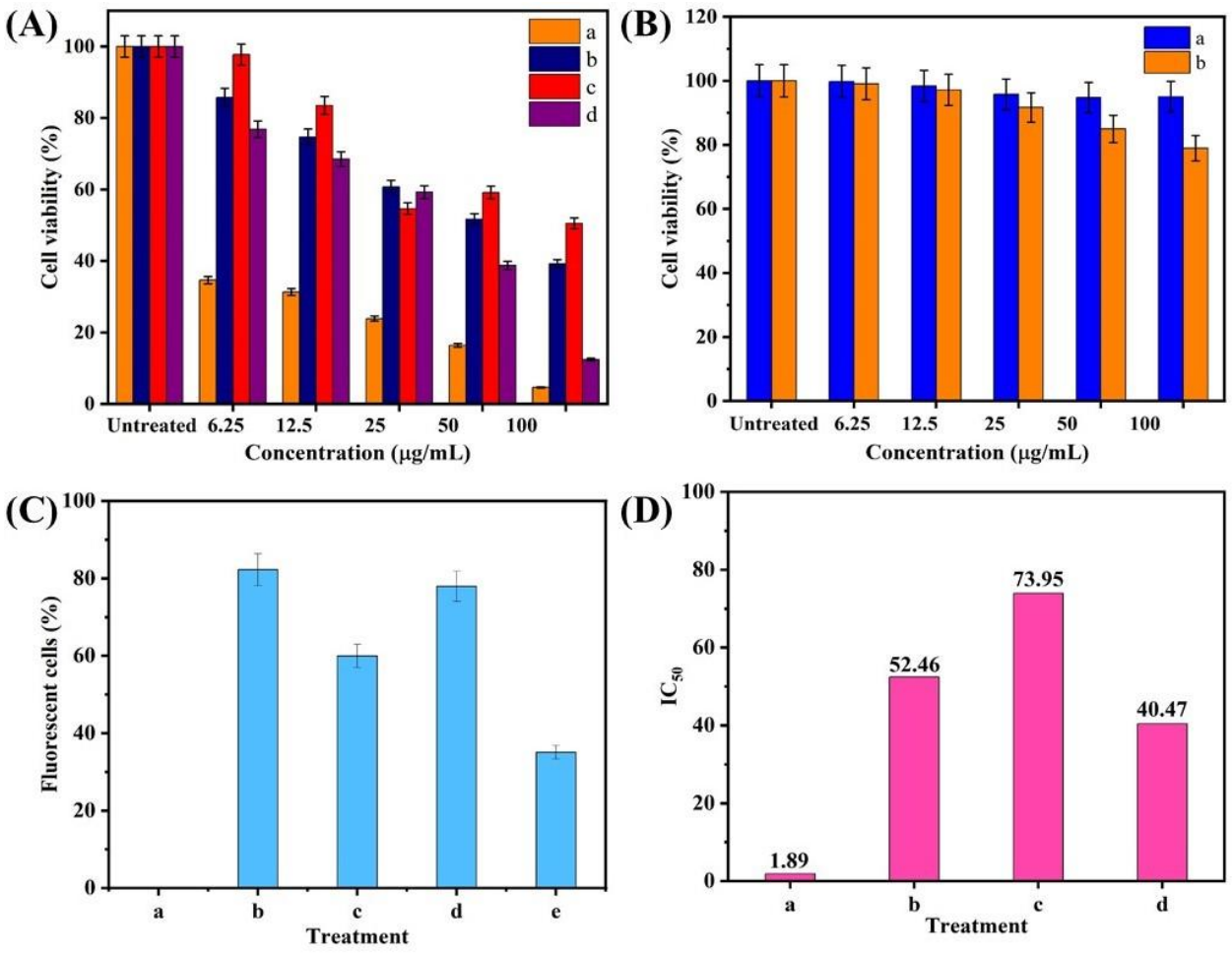

Figure 11. (A) Viability of MCF-7 cells after treatment with (a) DOX, (b) SAMC-DOX, (c) SAMC-ANPs-DOX, and (d) SAMC-ANPs**.** (B) Viability of MCF-10A cells after treatment with (a) SAMC and (b) ANPs**.** (C) ROS generation in MCF-7 cells after different treatments: (a) no treatment, (b) treatment with DOX, (c) treatment with SAMC-DOX, (d) treatment with SAMC-ANPs-DOX, and (e) treatment SAMC-ANPs. (D) The inhibitory concentration 50 (IC_{50}) values of (a) DOX, (b) SAMC-DOX, (c) SAMC-ANPs, and (d) SAMC-ANPs-DOX.

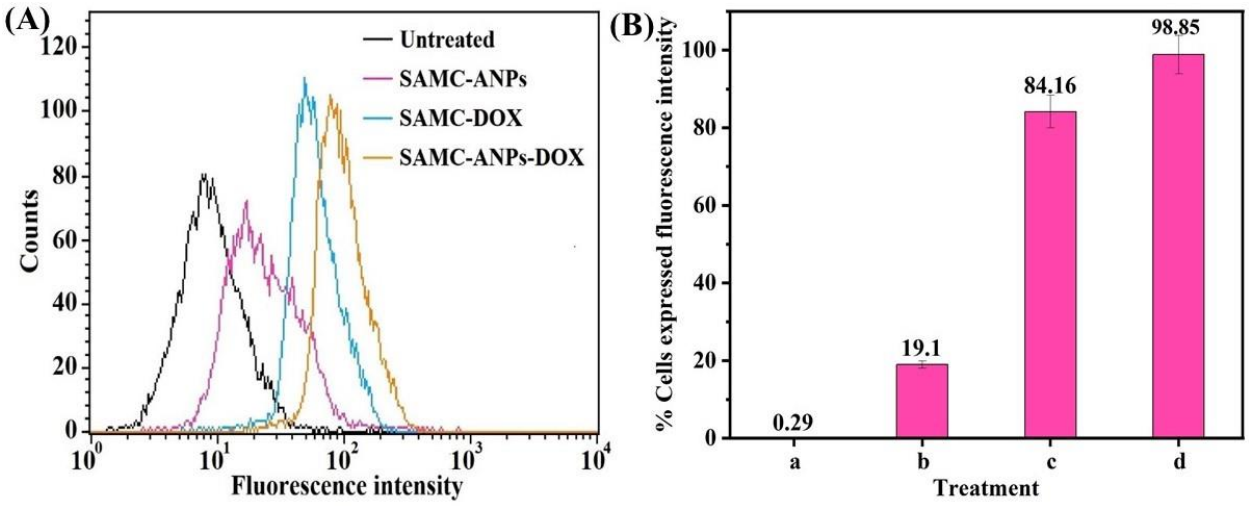

Figure 12. (A) Flow cytometry analysis of cellular uptake of ANPs and/or DOX released from different gel beads. (B) Quantitative analysis of the intensity of fluorescence exhibited by MCF-7 cells after different treatments: (a) no treatment, (b) treatment with SAMC-ANPs, (c) treatment with SAMC-DOX, (d) treatment with SAMC-ANPs-DOX

Table 1. Composition of different composite gel beads

	SA (mg)	MC (mg)	Water (mL)	ANPs (mg)	DOX (mg)
SAMC	200	200	20	0	0
SAMC-DOX	200	200	20	0	100
SAMC-ANPs	200	200	20	100	0
SAMC-ANPs-DOX	200	200	20	100	100

Table 2. Release kinetics parameters of different composite gel beads at pH 2.0 and 7.4 at 37 ^{o}C.

Formulation	pH	Zero order		First order		Higuchi		Korsmeyer-Peppas	
		K_0	r^2	K_1	r^2	K_H	r^2	n	r^2
SAMC-DOX	7.4	4.967	0.2466	0.181	0.9319	21.396	0.8688	0.9778	0.489
	6.4	4.195	0.3833	0.104	0.8478	17.943	0.8864	0.9588	0.546
	2.0	1.551	0.0487	0.019	0.2240	6.711	0.8384	0.9843	0.407
SAMC-ANPs-DOX	7.4	4.374	0.5422	0.107	0.9301	18.487	0.9416	0.9929	0.592
	6.4	3.817	0.5510	0.078	0.8729	16.126	0.9312	0.9825	0.618
	2.0	1.322	0.1909	0.016	0.3205	5.676	0.8872	0.9840	0.405